

# We are IntechOpen, the world's leading publisher of Open Access books Built by scientists, for scientists

6,900

Open access books available

186,000

International authors and editors

200M

Downloads

Our authors are among the

154

Countries delivered to

TOP 1%

most cited scientists

12.2%

Contributors from top 500 universities



WEB OF SCIENCE™

Selection of our books indexed in the Book Citation Index  
in Web of Science™ Core Collection (BKCI)

Interested in publishing with us?  
Contact [book.department@intechopen.com](mailto:book.department@intechopen.com)

Numbers displayed above are based on latest data collected.  
For more information visit [www.intechopen.com](http://www.intechopen.com)



# Biodegradable Chitosan Matrix Composite Reinforced with Titanium Dioxide for Biocidal Applications

*Johnny López Calero, Zuleika Oquendo Berríos and Oscar M. Suarez*

## Abstract

Access to drinkable water is increasingly difficult in developing nations. According to the World Health Organization, more than 1.2 billion people lack access to this resource. The scientific community has risen to the challenge by developing innovating methods to purify water. In this context, a chitosan/titanium dioxide biocomposite represents an appealing, economically viable solution to remove oils, heavy metals, and pathogen colonies from contaminated waters. The present chapter reports the study of a chitosan film matrix impregnated with nanoparticles, which was capable of expressing antibacterial properties when exposed to UV light. Several techniques allowed characterizing the biocomposite uniformity, corroborating the crystal structure and assessing the bonding type of this biocomposite mixture. Antibacterial tests with *Escherichia coli* (Gram-negative) and *Staphylococcus aureus* (Gram-positive) were completed via growth curve analysis and the Kirby-Bauer technique. The results of this encompassing study revealed that bacterial growth was reduced by more than 50%. Optical microscopy, Fourier-transform infrared spectroscopy, and X-ray diffraction helped to characterize this biocomposite film. This chapter discusses how a novel and biodegradable film represents a better antibacterial material that is able to eliminate pathogens cost-effectively.

**Keywords:** chitosan, titanium dioxide, anatase, *Escherichia coli*, *Staphylococcus aureus*, composite, biocide

## 1. Introduction

The widespread use of antibiotics has promoted the dissemination of multidrug resistance (MDR) genes in bacteria, whereas nanoparticles (NPs) have proven to be effective when dealing with this bacteria type [1]. Superbugs (i.e., bacteria which are resistant to nearly all antibiotics) have evolved due to the abuse, misuse, and negligence of antibiotics. They are capable of transferring their resistance by mechanisms as plasmid [2], transposon [3], and integrons [4]. This means that just one superbug can render an infection nearly untreatable. Antibiotics target mainly three areas inside bacteria: the cell wall, the translational machinery, and the DNA replication system. Superbugs can develop genes capable of resisting the effect of

antibiotics, ranging from the expression of enzymes and modification of cell components all the way to the creation of efflux pumps [5]. For example, enzymes such as  $\beta$ -lactamase [6] could alter the chemical structure of the antibiotics, leaving them inactive. Meanwhile, cell components such as ribosomes [7] offer resistance and efflux pump work by removing antibiotics from the inside of a cell and maintaining a safe environment for which the bacteria can grow normally.

Furthermore, NPs work differently when it comes to dealing with bacteria; this makes any antibiotic resistance ineffective against NPs. The NP antimicrobial mechanism falls into three categories: oxidative stress induction [8], metal ion release [9], and nonoxidative [10]. These mechanisms all work toward producing bacterial cell death.

Nanoparticles, as nanostructured materials, can be defined as three-dimensional materials with dimensions in the nanoscale (1–100 nm). As many studies suggest, they offer an array of antibacterial properties against Gram-negative and Gram-positive bacteria, such as *E. coli* and *S. aureus*, respectively. For example, zinc oxide (ZnO) NPs are capable of inhibiting the growth of *S. aureus*, while silver NPs demonstrate antimicrobial activity against *E. coli* [11].

As mentioned above, there are three main mechanisms by which NPs produce apoptosis. One can summarize the entire process as follows: first, the disruption of bacterial cell membrane occurs, followed by (whenever possible) the production of reactive oxygen species (ROS), which induces the penetration of the bacterial cell to disrupt the intracellular mechanism needed by the bacteria to function properly. NPs can produce ROS by different mechanisms, but, in the scientific community, the photocatalytic hypothesis is most widely accepted.

MDR genes have proliferated to such an extent that they become a challenge for the existing resources to counteract them. Accordingly, investigations related to antibacterial materials have become mandatory to protect human lives.

Prior research demonstrated that separately chitosan and TiO<sub>2</sub> (anatase polymorph) possess antibacterial properties under ultraviolet light irradiation. This characteristic can clean water sources, which represents one of the main vectors used by bacteria to infect the human body.

Water has become a precious resource, causing the access to fresh and clean water to become a critical matter at a global scale. Nowadays, innovative methods must offer clean, fresh, and purified water. As mentioned above, in this context, chitosan and TiO<sub>2</sub> biocomposites could be an economically viable alternative to resolve this problem by removing oils, heavy metals, and pathogen colonies.

## 2. Bacteria

Because of their incidence in global health, this study centered on two types of bacteria: a Gram-negative and a Gram-positive one. Details of them are provided in the next sections.

### 2.1 *Escherichia coli*

*Escherichia coli* (*E. coli*) is a Gram-negative, rod-shaped, facultative anaerobic bacterium, as shown in **Figure 1**. The cell wall consists of an outer membrane with lipopolysaccharide and peptidoglycan along with a plasma membrane. A good analogy is that this type of bacteria bears both an outer and an inner skin that offer double protection against foreign agents. Theodor Escherich first described this microorganism in 1885, making it one of the most studied bacteria in the world. *E. coli* strains colonized the gastrointestinal tract of humans and animals as a normal

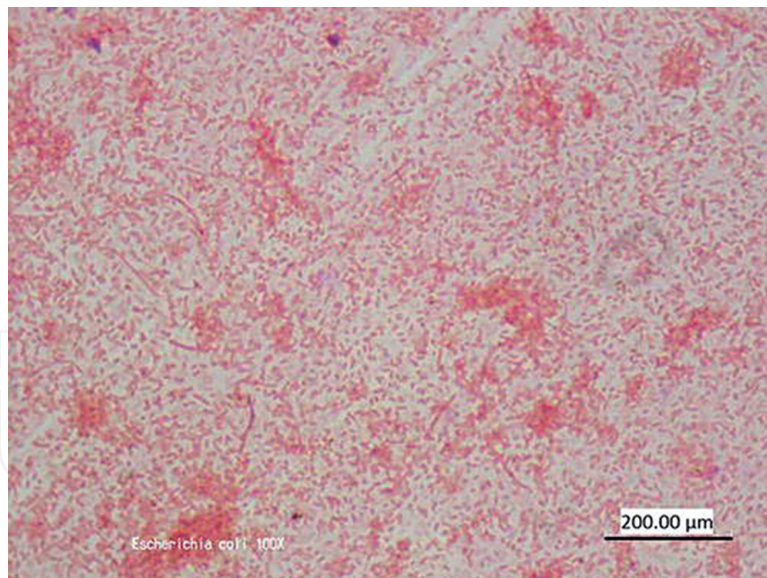


**Figure 1.**  
Optical image of *E. coli* stained using Gram's method.

flora [12]. Despite this, some strains have evolved into a pathogenic *E. coli*. This bacterium acquires virulence factors through transposons, bacteriophages, plasmids, and other pathogenicity islands. One can categorize *E. coli* as a pathogen, according to the pathogenicity mechanisms and clinical symptom serogroups or through virulence factors [12].

There is a variety of foods and environmental sources for the *E. coli* to grow that are resistant to a breadth of antimicrobial drugs, usually used in medicine and agriculture. Their particular resistance to antibiotics is of great importance, because these are Gram-negative pathogens commonly found in humans. For instance, there are different sources of contamination of vegetables, such as poor water treatment and the presence of fertilizers used during cultivation. Similarly, water or food contaminated with wastes can infect animals. Another vector of contamination is via meat products as a result of improper handling and processing or lack of hygiene [13].

There are numerous serotypes in enterohemorrhagic *E. coli* (EHEC) that are frequently associated with human diseases such as O26:H11, O91:H21, O111:H8, O157:NM, and O157:H7 [12]. *E. coli* O157:H7 is the most common isolated serotype of *E. coli*. It has been frequently isolated from people in the United States, Japan, and the United Kingdom. The *E. coli* O157:H7 is also a common food-related pathogen leading to major worldwide health problems. This enterohemorrhagic pathogen can cause different clinical symptoms ranging from diarrhea to death.

## 2.2 *Staphylococcus aureus*

*Staphylococcus aureus* (*S. aureus*) is also a common bacterium in the human body. This Gram-positive bacterium possesses a cell wall bearing only a thick peptidoglycan layer followed by a plasma membrane, as shown in **Figure 2**. It is present in the mucous membranes (nose) and in the skin [14]; 30% of healthy adults have these bacteria in the nose, and about 30% has it in the skin [15]. These percentages are increased in people who work in hospitals. *S. aureus* is spread by contact with infected people or by contact with contaminated objects.

Some common infections caused by *S. aureus* are:

- Pneumonia that causes fever, shortness of breath, and cough, causing abscesses in the lungs and accumulation of pus

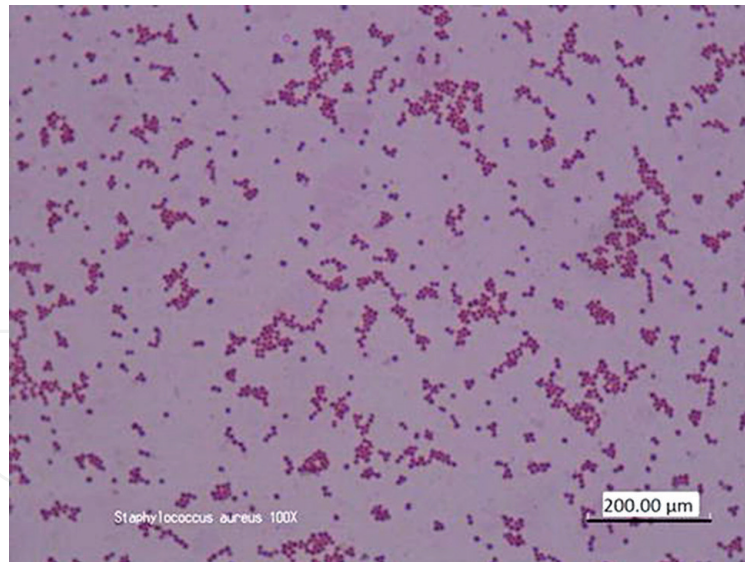


**Figure 2.**  
*Optical image of S. aureus stained using Gram's method.*

- Toxic epidermal necrolysis: infection that causes detachment of large amounts of skin
- Blood flow infection that produces high and persistent fever and shock
- Osteomyelitis: infection of the bones that can reach the bone through the bloodstream or can spread through the surrounding tissue

UV radiation can inhibit the bacteria growth. This is commonly used in medicine to sterilize surgical instruments. UV radiation kills the bacterium by disrupting its reproduction mechanism [16].

### 3. Chitin and chitosan overview

In recent years, the use of biopolymers has increased due to their broader application in cosmetics, pharmaceuticals, food industry, biomedical, agriculture, and environmental products. Chitin was discovered in 1811 by Braconnot and chitosan, in 1859, by Rouget [17]. Chitin is made of N-acetyl-D-glucosamine monomer units linked with  $\beta(1,4)$  glycosidic linkage, whereas chitosan is the deacetylated form of chitin [18]. In addition, chitosan presents a rigid crystalline structure due to inter- and intramolecular hydrogen bonds as a result of the amine and hydroxyl groups [18].

Chitosan is a long chain of hydrophilic polysaccharide with a chemical formula of  $\beta(1-4)$  2-asetamide-2-deoxy-D-glucopyranose. Chitosan is also known to be a natural polymer with similar molecular structure as cellulose; however it varies in the C-2 chain where the hydroxyl group in cellulose is replaced by amine ( $\text{NH}_2$ ). Chitosan is used to inhibit biofouling, being nontoxic and biocompatible, and also possesses inherent antimicrobial properties [19].

Chitin can be extracted from the exoskeletons of crustaceans and fungi by a two-step chemical processing: demineralization and deproteinization [20]. A wide variety of chemical processes allow preparing chitosan: solution casting, dipping and spray coating, compression molding, blending, layer-by-layer, and 3D printing [21].

Chitin along with chitosan is considered the most abundant natural polysaccharides after cellulose. Due to the abundance of waste of shrimps, crabs, and other

crustacean exoskeletons, chitin and chitosan are both a cost-effective and abundance product. As polymers, they can be shaped as membranes, films, nanofibers, capsules, tablets, microspheres, pastes, gels, powders, filaments, granules, sponges, and hydrogels. Biomedical uses of chitosan and chitin include drug delivery systems, tissue engineering, and wound healing, as a result of their extensive biocompatibility and biodegradability. For instance, chitosan can be degraded in vertebrates mainly by lysozyme and certain bacterial enzymes in the colon [22]. Moreover, chitosan presents a high in vivo biocompatibility and biodegradability with minimal inflammation and body reaction when applied as tissue [23]. Moreover, the film adhesion on tissue can induce the proliferation of fibroblasts, indicating high biocompatibility [23]. Despite the great biological properties, such as biocompatibility, nonimmunogenicity, antibacterial, and anti-tumorigenicity, there is a lack of sufficient knowledge on the regenerative mechanism of this biopolymer [24]. Another advantage is their functionalization, especially in the hydrophilic group, hydrophobic group, cationic group, targeting ligand, thiol group, and amino acid. This can lead to various gene therapy applications by improving their solubility, toxicity, buffering capacity, escapes in endosome, cellular uptake, genetic material release, transfection efficiency, and silencing efficiency [17]. Chitosan is also known for its anti-inflammatory effects on in vivo tissue applications, which can be applied to inhibit growths of Gram-positive and Gram-negative bacteria. Acting alone, chitosan has shown much promise in wastewater treatment, as it can be used in the removal of dyes, odor, organic pollutants, and inorganic heavy metal ions from industrial wastewater [21]. It can also be applied as an antifouling material used on boat paint because of its prevention on bacteria formation [25]. A problem is that parameters such as molecular weight of chitosan, acetic acid concentration, sterilization process, thickness of the matrix, pH of the medium, and cell parameters (i.e., age, concentration, and bacteria type) led to important differences on microbial growth [18].

#### 4. Titanium dioxide

Titanium dioxide has many commercially available applications in the food industry as a food additive, in the cosmetic industry as a makeup additive and sunscreen, and in the health industry as a drug delivery system [26]. It has also been used as a treatment of wastewater to remove pollutants [27]. Pure titanium dioxide when exposed to ultraviolet light (wavelength less than 400 nm) becomes a photocatalytic material [28]. This is largely dependent on particle size, shape, surface characteristics, and the dioxide crystal structure [29]. Different TiO<sub>2</sub> crystal structures (viz., anatase, rutile, and brookite) have different photocatalytic properties [29]. Sayes et al. demonstrated that the anatase polymorph is more reactive under ultraviolet light (UV) [30], which renders it more cytotoxic. Furthermore, Blinova et al. stated that pure anatase induces apoptosis but does not generate ROS, while rutile does initiate cell death through the formation of ROS [31]. Davis et al. proposed that anatase particles under 100 nm have a strong UV absorption [32].

Nevertheless, TiO<sub>2</sub> is a proven photocatalytic material under UV light. When this energy is greater than the band gap, i.e., 3.06 eV for rutile and 3.23 eV for anatase [33], the electrons in the valence band (VB) are excited to the conductive band (CB), producing a corresponding hole in the valence band and highly reactive reactants (e<sup>-</sup> and h<sup>+</sup>) on the TiO<sub>2</sub> surface, as shown in **Figure 3**.

The electrons and holes react with water and air to form the highly chemical active ROS. There are four main and common ROS: superoxide radical (O<sup>2-</sup>), hydroxyl radical (OH<sup>-</sup>), hydrogen peroxide (H<sub>2</sub>O<sub>2</sub>), and singlet oxygen (O<sup>-</sup>) [34]. They range from less acute (O<sup>2-</sup> and H<sub>2</sub>O<sub>2</sub>) to more acute (O<sup>2-</sup> and O<sup>-</sup>) [34]. Not all

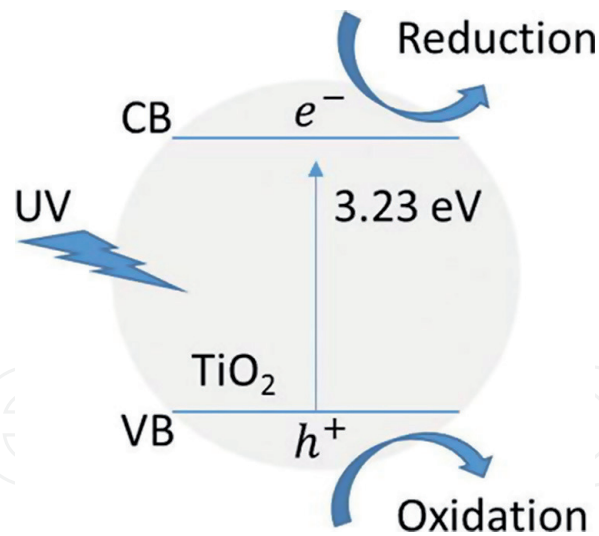
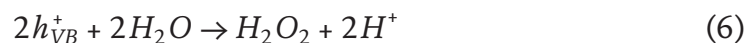


**Figure 3.**  
Schematic illustration for the photocatalytic reaction of  $\text{TiO}_2$ .

NPs can produce ROS, and even if they could, many do not produce them all. For example, calcium oxide (CaO) and magnesium oxide (MgO) NPs can only produce  $\text{O}^{2-}$  [34]. ZnO can generate  $\text{H}_2\text{O}_2$  and  $\text{OH}^-$  but not  $\text{O}^{2-}$  [34], while  $\text{TiO}_2$  and copper oxide (CuO) NPs can produce all four types of ROS [34]. For the sake of simplicity, the present work focuses only on  $\text{TiO}_2$  irradiated with UV light and is used as a ROS source.

Such ROS production induced by the irradiation of  $\text{TiO}_2$  with UV light is shown in the following equations. Eq. (1) describes the energy absorption and the photocatalytic reaction. Eqs. (2)–(4) depict the photocatalytic redox pathways involved in the generation of an  $\text{O}^{2-}$  and an  $\text{OH}^-$  at the reaction between the holes with  $\text{H}_2\text{O}$  and the electrons with  $\text{O}^{2-}$  [35]. Eqs. (5), (6) describe the generation of  $\text{H}_2\text{O}_2$  by reductive and oxidative pathways, respectively.



#### 4.1 Oxidative stress

The ROS formation is an oxidative stress mechanism due to the generation of an imbalance between the production of free radicals and the ability of the cell to counteract. Different bacteria have particular ways to protect themselves to some

degree against ROS. However, any overproduction of this species initiates a systematic failure that starts by damaging the cell component and ends with the cell death. Human cells are not exempt from the effect of ROS [36], due to their self-production in the mitochondria.

In bacteria the reactive oxygen species attack the cell membrane and proteins, affecting the interaction between deoxyribonucleic acid (DNA) and cell and increasing the gene expression for oxidative proteins [37]. Several studies found that the expression of two oxidative stress genes (catalase Kat A and alkyl hydroperoxide reductase, Ahp C) and a general stress response gene (chaperon protein, DNA K) rose by 52, 7, and 17 times, respectively, as revealed by real-time polymerase chain reaction (RT-PCR) [38].

Negatively charged  $O^{2-}$  and  $OH^-$  can exist on the cell surface and cannot penetrate the intracellular regions of the bacteria because of the negative charge barrier; conversely, hydrogen peroxide [39] can easily pass through. Therefore, NPs that produce all ROS have a higher opportunity as a broad-spectrum biocide. Furthermore, there exists evidence that  $TiO_2$  increases the membrane permeability of a bacterial cell, which allows ROS to enter and start the cell death process [40].

## 5. Methodology

### 5.1 Materials

For the production of the biocomposite, the following materials were used: chitosan powder (coarse ground flakes, deacetylated chitin, poly(D-glucosamine) CAS number: 9012-76-4), acetic acid (glacial ACS reagent (2.5 L, RABA0010–2.5D1)), and  $TiO_2$  (anatase polymorph) purchased from Sigma Aldrich® now Millipore Sigma® (22 nm, nanocrystalline colloidal paste for transparent films, >95% anatase by x-ray diffraction, 60–65% porosity, specific surface area 65–75  $m^2$ , pH <1, #798495).

To test the antibacterial properties of this renewable biocomposite, *E. coli* (ACTC 25922) and *S. aureus* (ATCC25923), provided by the Biology Department at the University of Puerto Rico—Mayagüez (UPRM), were used. The bacterial medium used to grow them was the Miller's Luria Broth (LB, CAS number: 91079–40-2, tryptone 10 g/L, yeasts 5 g/L, and sodium chloride 10 g/L), provided by Research Product International (RPI). An in-house Millipore filter provided the necessary deionized water. To provide aseptic conditions and for disinfection, common Lysol® diluted in distilled water was used. The use of protective gear, i.e., face masks, laboratory coats, gloves, and safety glasses, was mandatory throughout the entire experimental work. Laboratories in the UPRM Biology Building and Stéfani Building hosted the present research.

### 5.2 Chitosan/ $TiO_2$ film production

Following the procedure for polymer solution casting, we measured and mixed chitosan powder with acetic acid and deionized water following this schedule: a mechanical agitator for 1.5 h, a sonicator for 1 h, and a magnetic agitator for another 1 h. The  $TiO_2$  powder (anatase polymorph) was added in increments of 0.5 wt% to reach each target concentration and to prepare four different mixtures of  $TiO_2$  and chitosan. These mixtures were left inside an oven at 55°C for 48 hrs to be then utilized and characterized. **Figure 4** shows the as-produced films ready to be tested.

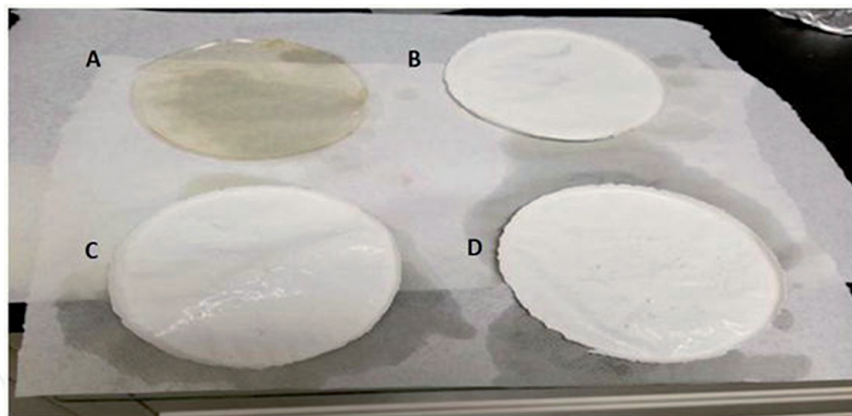


**Figure 4.** Films as extracted from the oven. (A) 0.0%  $\text{TiO}_2$ , (B) 0.5%  $\text{TiO}_2$ , (C) 1.0%  $\text{TiO}_2$ , and (D) 1.5%  $\text{TiO}_2$ .

### 5.3 Bacteria medium preparation for growth curve analysis

In this protocol, we prepared the bacterial medium of Luria broth (LB) nearly 24 h before each experiment. All laboratory glassware was autoclaved for 15 minutes before use. One liter of water was mixed with 10 g of LB assisted by a magnetic agitator. After obtaining a visually homogenous mixture, we divided it in three groups of laboratory plastic tubes, namely, control, *E. coli*, and *S. aureus*, and autoclaved a second time for 15 minutes. Each bacteria medium was left overnight inside a fume hood under UV light. Two master solutions were separated from the group, incubated with the bacteria, and left inside a shaker at 200 rpm and 37.0°C for almost 6 h. We followed this entire procedure twice per experiment to produce enough samples to be tested with and without UV.

## 6. Characterization

### 6.1 Growth curve analysis

Growth curve analysis (GCA) allowed assessing the effect of the ROS generated from the  $\text{TiO}_2$  upon UV irradiation. As mentioned, we tested two bacteria: *E. coli* and *S. aureus*. We removed the bacterial media from the hood (protocol described previously) and mixed them with the films impregnated with  $\text{TiO}_2$  in laboratory plastic tubes as shown in **Table 1**.

A spectrophotometer allowed measuring the optical density (OD) of each master solution for each bacterium so that one could extract a fixed amount of volume (aliquot) from the solution for each bacterium. This aliquot was then added and mixed to each laboratory plastic tube with the bacteria medium and biocomposite film, as mentioned above. To know exactly how much volume was needed, Eq. [7] was used. Eq. [7] related the volume needed ( $v_2$ ) of aliquot to add to each plastic tube.  $C_1$ ,  $C_2$ , and  $V_1$  are the concentration of the plastic tube, the concentration in the master solution, and volume of medium already in the plastic tube (20 mL), respectively. The concentration was obtained from the OD measurement.

$$V_2 = \frac{C_1 V_1}{C_2} \quad (7)$$

**Table 1** presents the three groups formed, i.e., the control group with only the composite films and the medium without bacteria, the group with *E. coli* and

Group	Number of laboratory tubes				
	<i>S. aureus</i>	<i>E. coli</i>	Control	TiO <sub>2</sub>	UV
Day 1	3	3	3	Yes	Yes
	3	3	3	No	Yes
Day 2	3	3	3	No	No
	3	3	3	Yes	No

**Table 1.**  
 The number of laboratory plastic tubes used and how the groups were organized.

films with bacteria medium, and the group with *S. aureus* and films with bacteria medium.

After the three groups were ready, we measured the OD after the first 20 minutes three times (20, 40, and 60 minutes) of the mix preparation, then after 40 minutes three times (100, 140, and 180 minutes), and, finally, after an hour five times (240, 300, 360, 420, and 480 minutes).

During the wait time, i.e., between measurements, the test tubes remained inside the shaker under optimal conditions for bacterial growth. It is important to understand that we completed this entire process twice. As UV light irradiated the samples, we covered the shaker with a black box to block any other light source. **Figures 5** and **6** show how the films without any UV irradiation affected the bacteria growth.

**Figures 5** and **6** prove the negligible antibacterial capacity of the films without photoactivation (no UV light). As we can observe in both **Figures 5** and **6**, the samples with bacteria grow normally (if we compared the sample with only bacteria with the samples of bacteria and films), while the samples without bacteria stay constant (0.0 absorbance) until close to the end of the experiment. The samples are either grouped on the top (samples with bacteria) or in the bottom (samples without bacteria). On the other hand, **Figures 7** and **8** (obtained for *S. aureus* and *E. coli*, respectively) have shown that the effect of photoactivated films becomes apparent. The growth rate reduction is attributed to the effects of the ROS liberated from TiO<sub>2</sub> when exposed to energy from the UV light.

**Figures 7** and **8** display a difference in the bacteria growth on the films photoactivated by UV. Further, **Figures 9** and **10** (obtained for *S. aureus* and *E. coli*, respectively) evince the difference in growth percent of the bacteria exposed to the

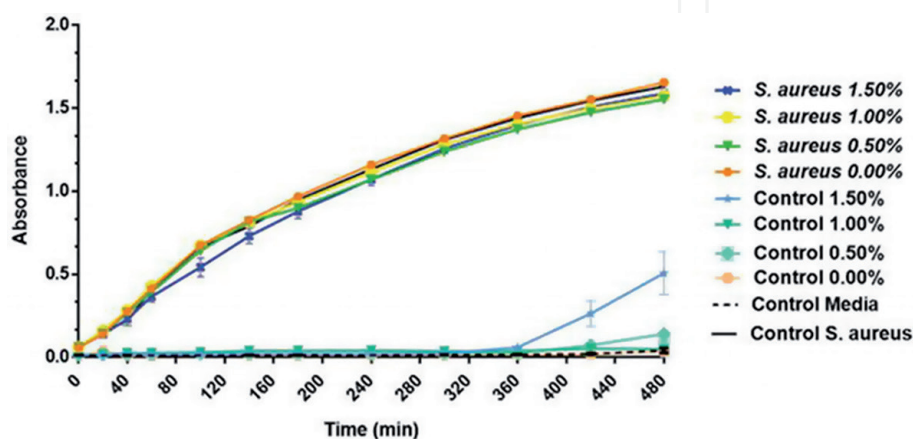


**Figure 5.**  
*S. aureus* exposed for 8 h to the chitosan films impregnated with TiO<sub>2</sub>, without UV irradiation. The upper curves indicate the presence of bacteria, while the bottom ones indicate lower bacteria content.

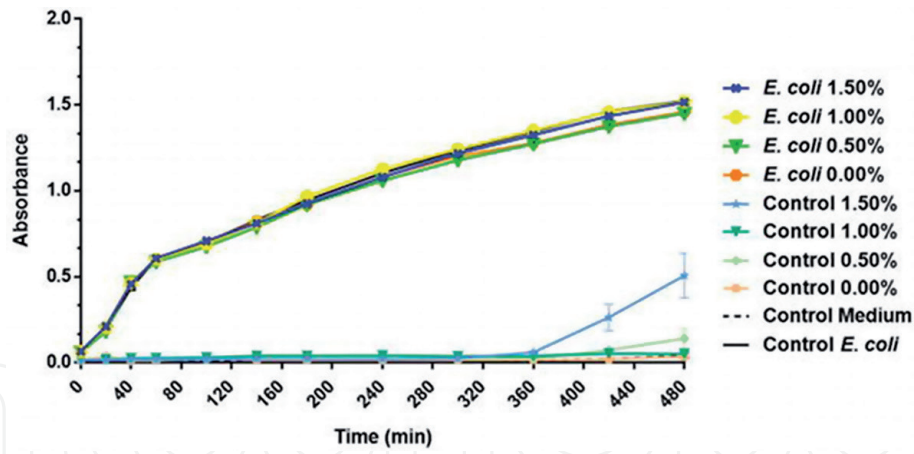


**Figure 6.** *E. coli* exposed for 8 h to the chitosan films impregnated with TiO<sub>2</sub>, without UV irradiation. The upper curves indicate the presence of bacteria, while the bottom ones indicate lower bacteria content.

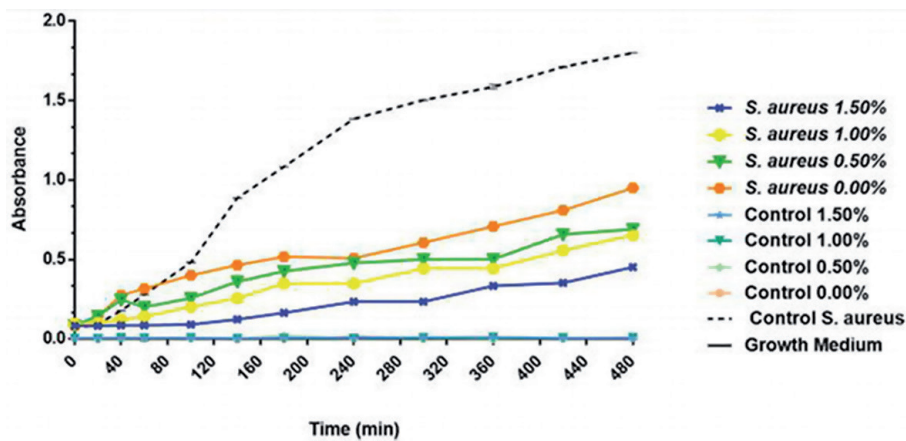


**Figure 7.** *S. aureus* exposed for 8 h to the chitosan films impregnated with TiO<sub>2</sub>, with UV irradiation.

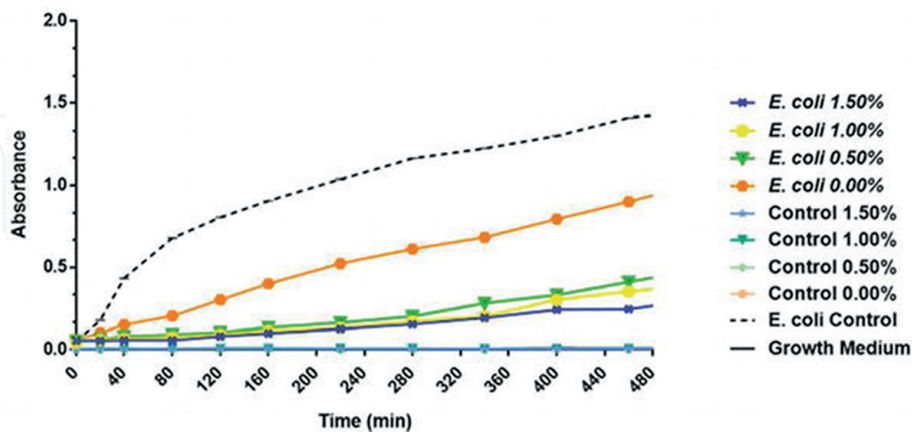


**Figure 8.** *E. coli* exposed for 8 h to the chitosan films impregnated with TiO<sub>2</sub>, with UV irradiation.

films after the growth rate stabilized at the end of the experiment. As observed in these two figures, the ceiling line corresponds to the normal growth of the bacteria. The bars represent the growth rate of each bacterium exposed to the different concentrations of TiO<sub>2</sub> in the films. **Figures 11** and **12** show the same bacteria groups exposed to the same level of TiO<sub>2</sub> but this time with UV light.

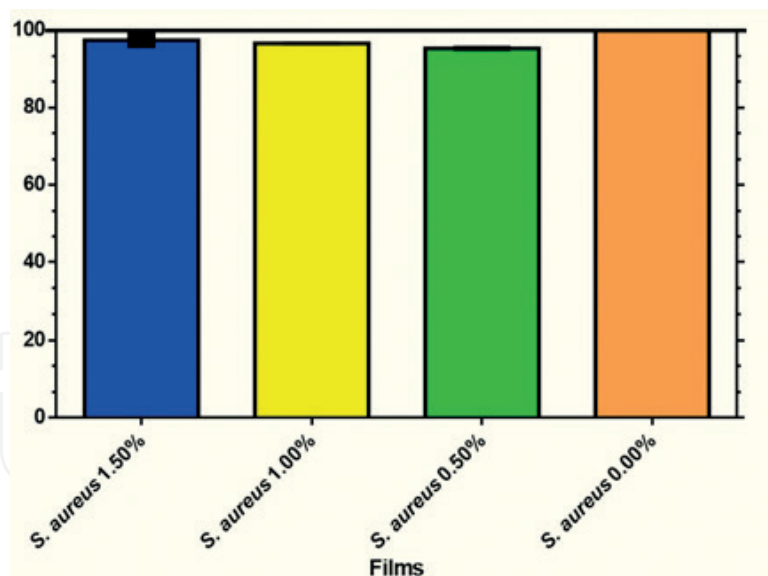


**Figure 9.**  
Growth percent of *S. aureus* exposed for 8 h to the biocomposite films made of chitosan and  $\text{TiO}_2$ .

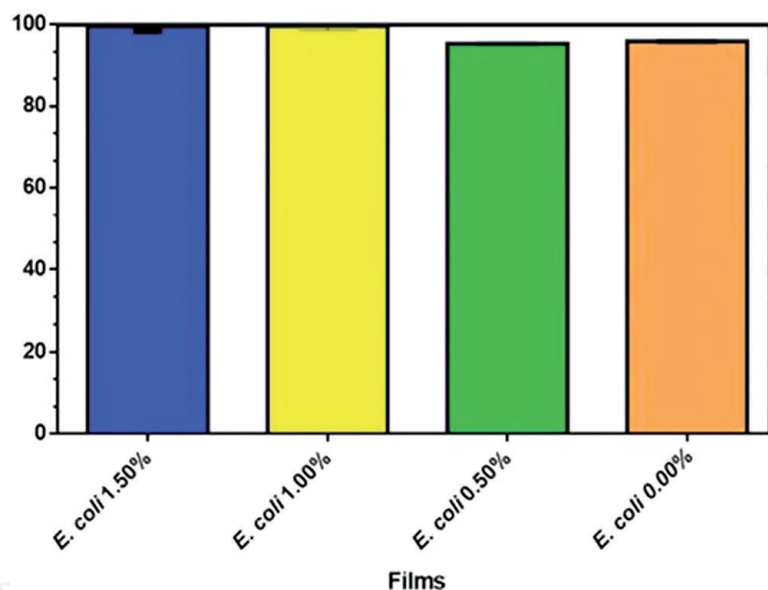


**Figure 10.**  
Growth percent of *E. coli* exposed for 8 h to the biocomposite films made of chitosan and  $\text{TiO}_2$ .

As observed in **Figures 9** and **10**, the ceiling line is the normal growth of the bacteria. The bars are the bacteria exposed to the different concentrations of  $\text{TiO}_2$  in the films. **Figures 11** and **12** (obtained for *S. aureus* and *E. coli*, respectively) show the same bacteria groups exposed to the same concentration of  $\text{TiO}_2$  but this time with UV light.

**Figures 11** and **12** demonstrate how the exposure of the films to the UV light did affect the bacteria growth. One can say that the UV light alone is detrimental to the bacteria but the experiments with only UV exposure did not affect the growth rate significantly.

## 6.2 Inhibition ring analysis

This analysis, also known as the Kirby-Bauer (KB) method, helps determine the susceptibility to solutions or drugs of isolated microorganisms, i.e., in our case *E. coli* and *S. aureus*. We cut the films as circular pieces using a paper perforator so

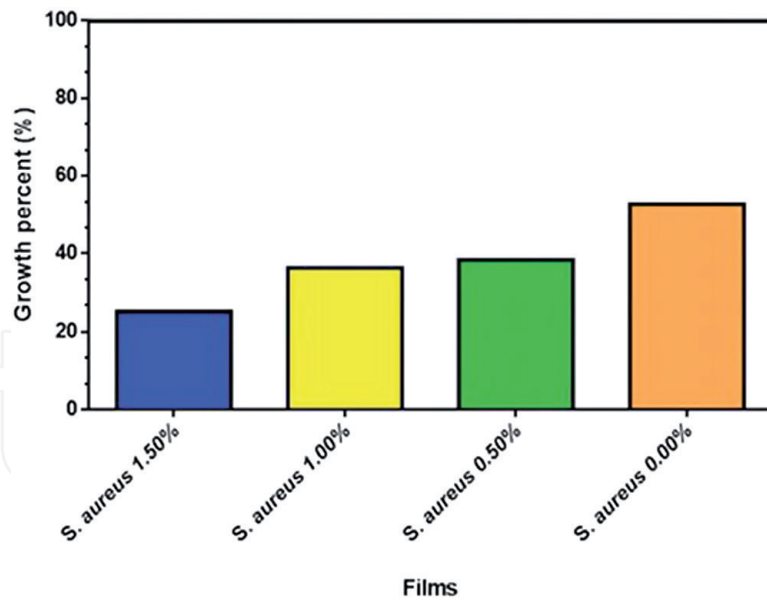


**Figure 11.** Growth percentage of *S. aureus* exposed for 8 h to the biocomposite films made of chitosan and TiO<sub>2</sub> with UV light.

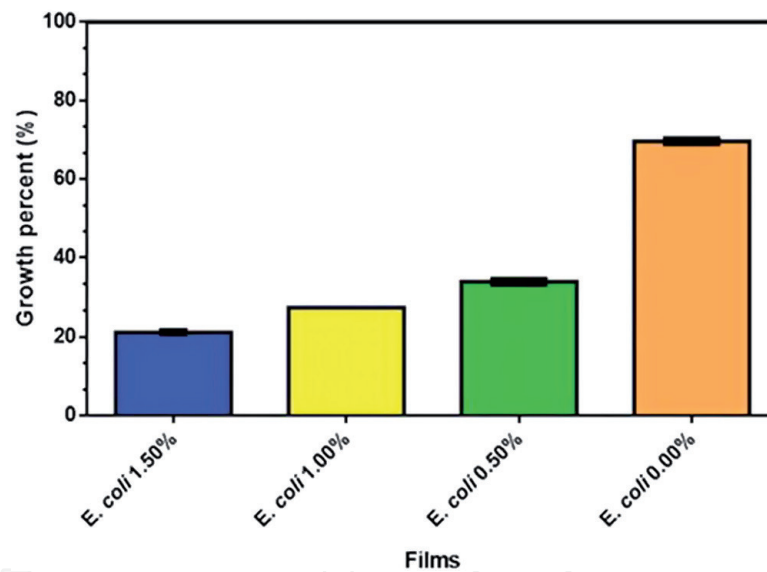


**Figure 12.** Growth percentage of *E. coli* exposed for 8 h to the biocomposite films made of chitosan and TiO<sub>2</sub> with UV light.

that all pieces had the same diameter. These were then exposed to UV irradiation for different times. The best results were obtained on films exposed to UV light for 168 h, as shown in **Figures 13** and **14**. When the UV exposure was over, we placed the films over the bacteria in the Petri dishes. Afterward, the bacteria would grow forming a ring along the chitosan piece with NPs. We measured the area of this ring as a measure of the biocidal potential of the biocomposite. In other words, a larger ring area represented better antibacterial properties of the material.

**Figure 13** shows four groups of *S. aureus*. Each group was exposed to a different film with different TiO<sub>2</sub> concentrations. The horizontal axis corresponds to the time elapsed after the films were placed over the bacteria. Naturally, at 0.00 h there was no inhibition ring yet since the films had just been placed on the bacteria.

Similar to **Figure 13**, **Figure 14** has the bacteria *E. coli* exposed to different concentrations of TiO<sub>2</sub>. The very first point after the films were placed was without inhibition rings yet. Here the optimal TiO<sub>2</sub> concentration was 1.0% and not 1.5%, which was to be expected due to the double membrane that the *E. coli* possesses.

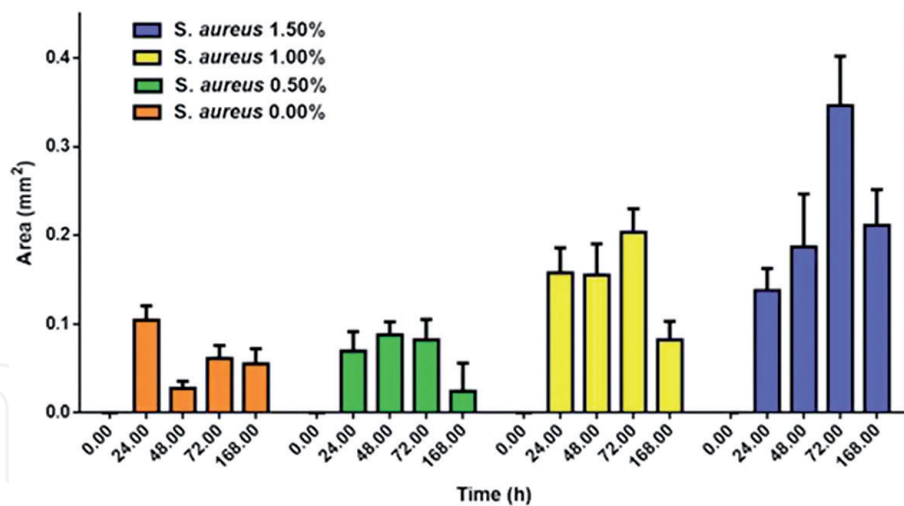


**Figure 13.** Area of inhibition ring for *S. aureus* after films are exposed for 168 h to UV light. Each bar was a different data point of the same plate taken continuously every 24 h.

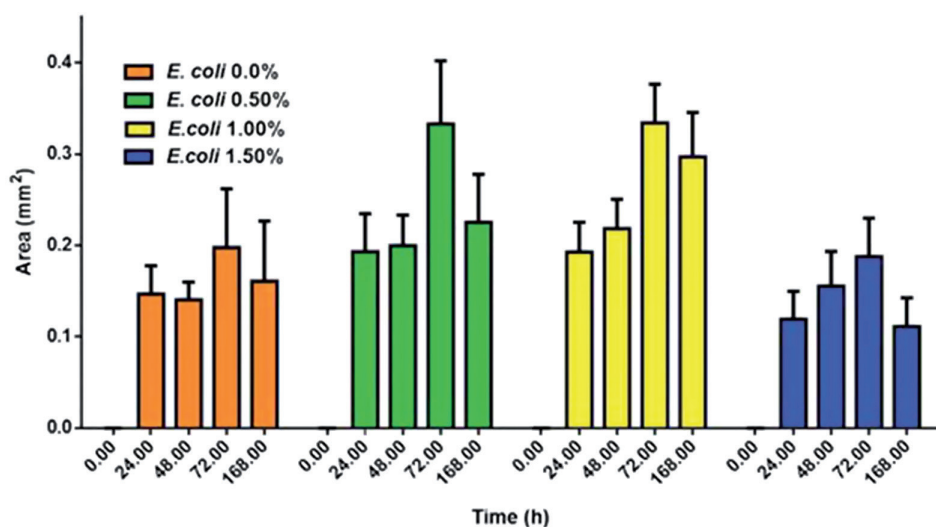


**Figure 14.** Area of inhibition ring of *E. coli* after films are exposed for 168 h to UV light. Each bar was a different data point of the same plate taken continuously every 24 h.

### 6.3 Fourier-transform infrared (FTIR)

The Fourier-transform infrared (FTIR) spectroscopy helps identify functional groups in a molecule. In our case, we used it to identify the chemical bonds present and how they degraded after UV exposure. As it is well-known, UV irradiation degrades the covalent bonds in polymers, rendering them brittle after a prolonged time under UV light.

In that context, FTIR spectroscopy, as a chemical analytical technique, helps measure the infrared intensity as a function of the wavelength (or wave number) of light. Based upon said wave number, infrared light can be categorized as far infrared, mid infrared, and near infrared for use in polymer science, organic synthesis, petrochemical engineering, food analysis, and even pharmaceutical industries [41, 42]. **Figures 15–18** show the results from four films after the UV exposure. Even more, by using the transmittance percent, we can detect the difference among films before and after such UV exposure.

The characteristic bands of 3400, 3000, 1080, and 1030  $\text{cm}^{-1}$  were assigned to the stretching vibration of O—H groups, C—H group, C—N groups, and C—O—C groups, respectively. The band at 1618  $\text{cm}^{-1}$  was attributed to the bending vibration of N-H.

A transmittance increment becomes evident after the UV light exposure on the films according to our results in **Figures 15–18**. The breakdown of the covalent bonds in the polymer reveals the degradation. Each valley is a different bond that when degraded absorbs less energy.

#### 6.4 X-ray diffraction (XRD)

X-ray diffraction (XRD) is a phase identification tool in crystal materials [43]. In the present study, XRD analysis allowed confirming the crystalline nature of the  $\text{TiO}_2$  used, identifying it as the anatase polymorph. A comparison between two diffraction patterns is in **Figure 19**. Further, this XRD analysis revealed that during the entire synthesis, process of the films (described in Section 5.2) did not affect the original anatase polymorph of the  $\text{TiO}_2$ . In effect, via **Figure 19**, we can conclude this because each peak (reflected by specific indexed crystallographic planes) aligns

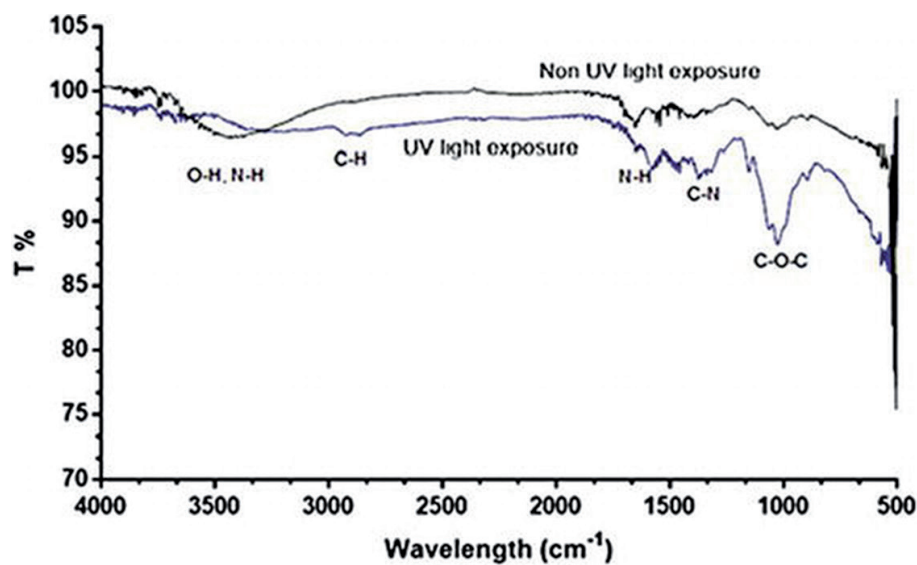


**Figure 15.** FTIR spectrum of the 0.0%  $\text{TiO}_2$  film after the UV exposure (blue line) for 24 h and without UV exposure (black line).

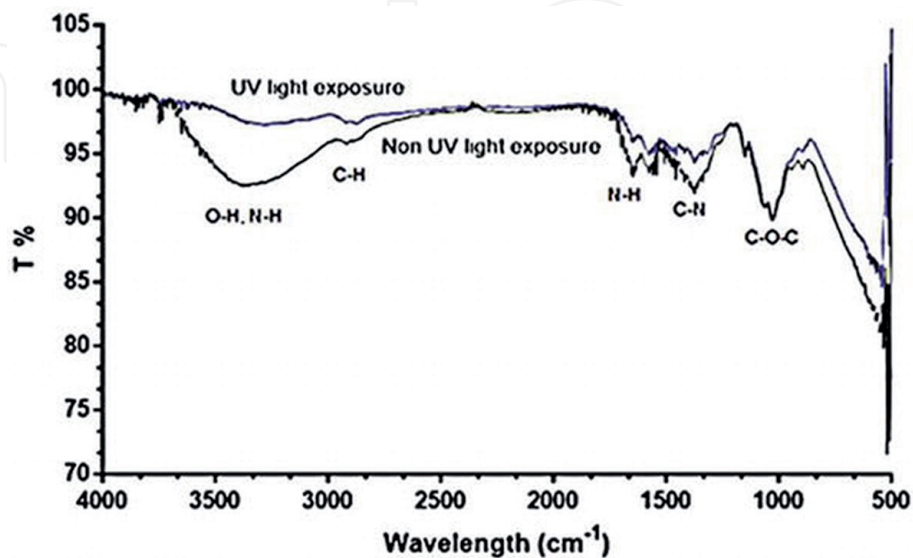


**Figure 16.** FTIR spectrum of the 0.5%  $\text{TiO}_2$  film after the UV exposure (blue line) for 24 h and without any exposure (black line).

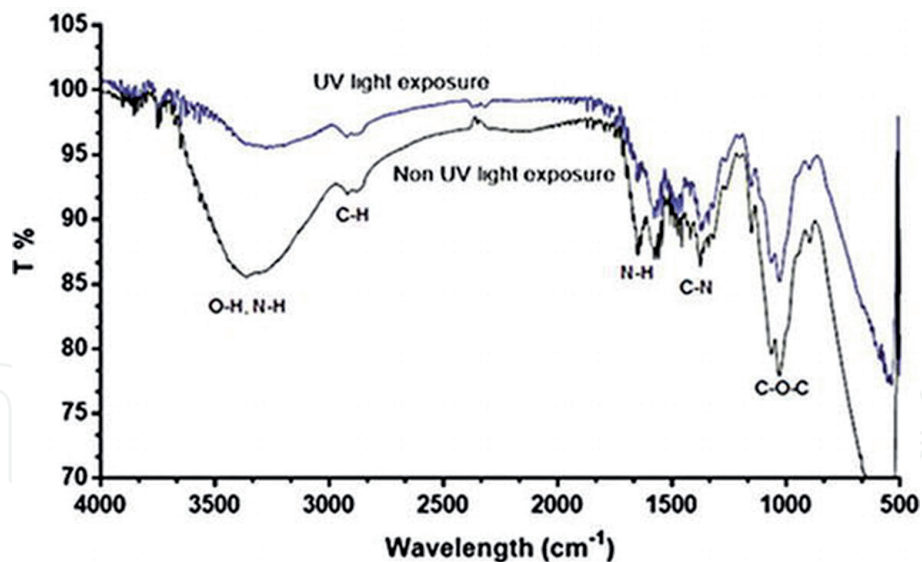


**Figure 17.**  
FTIR spectrum of the 1.0% TiO<sub>2</sub> film after the UV exposure (blue line) for 24 h and without any exposure (black line).

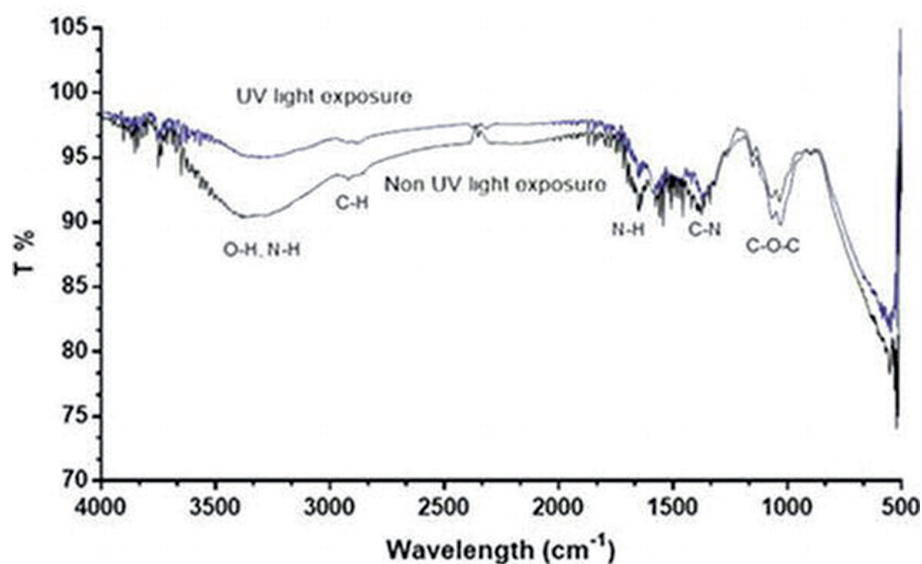


**Figure 18.**  
FTIR spectrum of the 1.5% TiO<sub>2</sub> film after the UV exposure (blue line) for 24 h and without any exposure (black line).

almost perfectly with the anatase pattern. This is an important finding since any formation of the two other polymorphs or even the amorphous alternative would have resulted in a loss of the photocatalytic capacity of the dioxide.

### 6.5 Scanning electron microscopy (SEM)

Scanning electron microscopy (SEM) helped acquire information about the external morphology (texture) of the films [44]. In this research, SEM confirmed the adequate TiO<sub>2</sub> dispersion within the chitosan matrix. **Figure 20** shows the 0.0% and 0.5% films with two (2) different positions and angle for each sample. **Figure 21** reveals analogous information for the films 1.0 and 1.5%. As the amount of NPs increased, the uniformity was maintained.

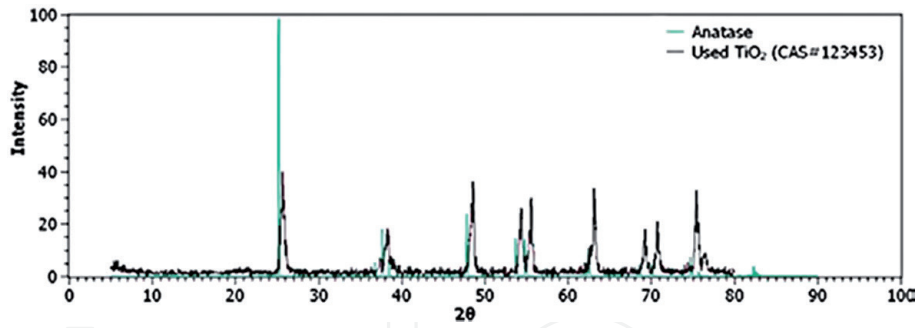


**Figure 19.** XRD analysis diffraction of the  $\text{TiO}_2$  used in the research, compared to pattern of anatase.

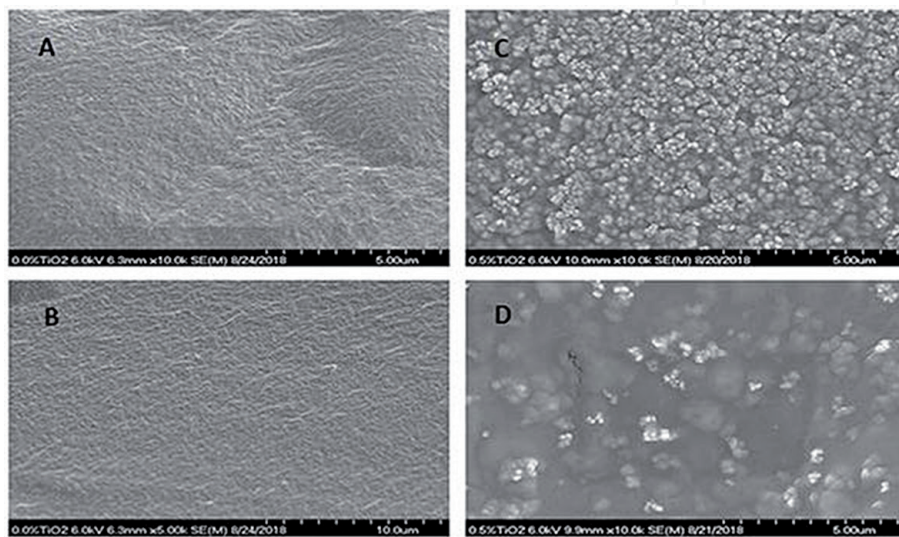


**Figure 20.** SEM images of the films containing 0.0%  $\text{TiO}_2$  (A, B) and 0.5%  $\text{TiO}_2$  (C, D).

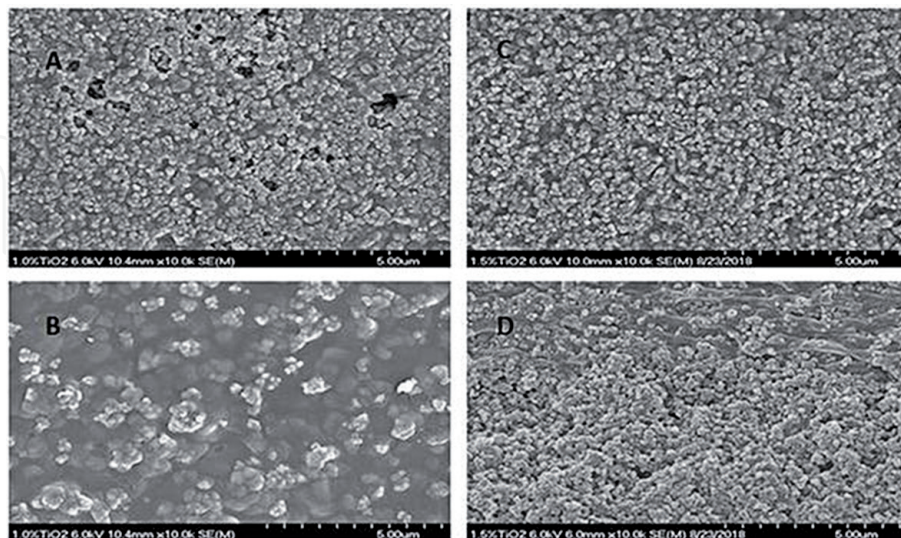


**Figure 21.** SEM images of the films containing 1.0%  $\text{TiO}_2$  (A, B) and 1.5%  $\text{TiO}_2$  (D, C).

For each film, multiple shots were taken at different angles and positions within the films. **Figures 20** and **21** present the most typical configurations of the particle dispersion. **Figure 20** A and B shows the surface of the chitosan without NPs. SEM analysis in overall

showed a uniform distribution of TiO<sub>2</sub> nanoparticle clots over the chitosan film as no large aggregate was observed. No phase separation was evident, as the TiO<sub>2</sub> content increased.

## 7. Discussion

As a whole, the results in Figures 5 through 12 prove clearly that the biocomposite film made of chitosan and TiO<sub>2</sub> NPs can be photoactivated. Once the films containing NPs have produced ROS, they are capable of reducing significantly the amount and growth rate of bacteria. Two different tests (*viz.*, the growth curve analysis and the Kirby-Bauer technique) present incontrovertible evidence that when the bacteria are exposed to the photoactivated biocomposites, their growth pattern is affected, and the end amount is lower. We already mentioned that the reviewed literature proved that the main mechanism affecting the bacteria growth is the production of ROS rendered by the TiO<sub>2</sub> upon UV light irradiation. However, in order for these ROS to be effective (in sufficient concentration), the correct polymorph of TiO<sub>2</sub> is needed, *i.e.*, anatase. For this reason, we selected this dioxide NPs, seeking to obtain more ROS, as mentioned in Section 4 of this chapter. Nonetheless, it is well-known that different processing conditions (involving temperature) of titanium dioxide can lead to a phase change. Thanks to the XRD characterization, we were able to confirm that the crystal structure used throughout this research was anatase and that the synthesis process of the biocomposite films did not change its crystal structure.

During the said process, the mixing methods used to disperse uniformly the TiO<sub>2</sub> NPs in the chitosan could have caused clots and agglomeration of the particles. This was the only reason to use a SEM (secondary imaging mode) to acquire the images shown in Section 6.5. The technique allowed scrutinizing the entire film exposed surface from different angles. This extensive survey did not evince any large clots or even lumps of NPs on the surface of the films. These images also proved that the attachment of the NPs onto the chitosan films was efficacious. In effect, as the TiO<sub>2</sub> content increased more, film surface was uniformly covered by the NPs, and no detachment occurred.

To reveal the interaction between TiO<sub>2</sub> and chitosan before and after UV irradiation, as already presented in Section 6.3, we acquired a set of FTIR spectra. Due to the addition of oxygen atoms from the TiO<sub>2</sub> NPs, one can observe a more intense peak from the O-H bond in **Figures 16–18**. Along that line, as the UV light photoactivated the TiO<sub>2</sub>, the spectral data revealed a smaller intensity from this bond (O—H) after the UV irradiation. Finally, the bond nigh 3000 cm<sup>-1</sup> (C—H) indicates a degradation of the chitosan polymer as this peak decreases. This could result in a more brittle substrate to hold the nanoparticles, which should be taken into consideration in upcoming applications of the composite.

In closing, even with the rise of superbugs and the decline in effectiveness of antibiotics, innovated materials like nanoparticles show a promising future as the next generation of antimicrobial. In this context, our chitosan/TiO<sub>2</sub> biocomposite films can represent an economic option when compared to other materials for similar applications, such as activated carbon, capable of reducing the bacteria present in water. The synthesis process is reproducible and very economical, creating a technology with ample potential application.

## 8. Conclusions

This chapter presents an appealing alternative of a novel antibacterial material. The use of chitosan was due to its versatility, its abundance in nature, and excellent

biocompatibility and nontoxicity. Through a straightforward technique, TiO<sub>2</sub> nanoparticles dispersed onto a chitosan matrix permitted formulating a renewable and biodegradable composite film capable of excellent antibacterial properties when exposed to UV light.

The synthesis process used did not affect the crystal structure of the dioxide, which remains anatase polymorph. X-ray diffraction characterization confirmed such anatase structure.

Chitosan demonstrated to be a very good selection as a matrix able to hold in place the TiO<sub>2</sub> nanoparticles. Incorporation of TiO<sub>2</sub> nanoparticles onto the chitosan film via solution casting method produced the chitosan/TiO<sub>2</sub> biocomposite films. The immobilized TiO<sub>2</sub> exhibited good distribution in the chitosan film, as demonstrated via secondary electron microscopy. From those observations, one can infer that chitosan provides an excellent substrate to immobilize TiO<sub>2</sub> nanoparticles. Electron microscopy also demonstrated that the nanostructured TiO<sub>2</sub> particles dispersed homogeneously within the polymer matrix without obvious aggregation even at the highest TiO<sub>2</sub> content, i.e., 1.5% wt.

Under UV light, TiO<sub>2</sub> proved effective against *E. coli* and *S. aureus*. This is due to the generation of ROS from the UV excitement of the TiO<sub>2</sub>. The growth curve analysis demonstrated that the growth rate of bacteria was affected, as evidenced by the Kirby-Bauer technique. In the present experimental conditions, the best effect came from biocomposites containing 1.5% wt TiO<sub>2</sub>.

The irradiation with UV light affected the chitosan covalent bonds, as revealed by the Fourier-transform infrared spectroscopy. From the spectra of chitosan with TiO<sub>2</sub>, one could infer that more oxygen molecules were present. The degradation of the bond at 3000 cm<sup>-1</sup> (C—H) demonstrated that extensive UV light irradiation is detrimental to the biopolymer, compromising its integrity in actual applications.

The research presented for the synthesis of the films is an effective way to immobilize TiO<sub>2</sub> while retaining the structure of the stronger photocatalytic polymorph.

## Acknowledgements

This material is based upon work supported by the National Science Foundation under grants No. 0851449 and 1345156 (CREST Program). The authors would like to thank Ms. Barbara Sanchez along with the UPRM Biology Department for the use of their facilities. Professor Matias Cafaro provided insightful comments for the completion of this research.

## Conflict of interest

The authors declare no conflict of interest.

## Notes/thanks/other declarations

Most of the work completed in the laboratory was with the assistance of the following undergraduate students: Amanda Quintero, Yamalis Lopez, Christian McRobert, Katyria Torres, Kenneth Serrano, Karimar Amador, Ariana Torres, Luis Orta, Genesis Reyes, Luis Olmo, Karla Romero, and Edwin Ramos.

IntechOpen

IntechOpen

### **Author details**

Johnny López Calero, Zuleika Oquendo Berríos and Oscar M. Suarez\*  
University of Puerto Rico at Mayagüez, Mayagüez, Puerto Rico

\*Address all correspondence to: [oscarmarcelo.suarez@upr.edu](mailto:oscarmarcelo.suarez@upr.edu)

### **IntechOpen**

---

© 2019 The Author(s). Licensee IntechOpen. This chapter is distributed under the terms of the Creative Commons Attribution License (<http://creativecommons.org/licenses/by/3.0>), which permits unrestricted use, distribution, and reproduction in any medium, provided the original work is properly cited. 

## References

- [1] Hsueh P-R. New Delhi metallo- $\beta$ -lactamase-1 (NDM1): An emerging threat among enterobacteriaceae. *Journal of the Formosan Medical Association*. 2010;**109**:685-687
- [2] Coetzee J, Corcoran C, Prentice E, Moodley M, Mendelson M, Poirel L, et al. Emergence of plasmid-mediated colistin resistance (MCR-1) among *Escherichia coli* isolated from South African patients. *South African Medical Journal*. 2016;**106**(5):449-450
- [3] Tsutsui M, Kawakubo H, Hayashida T, Fukuda K, Nakamura R, Takahashi T, et al. Comprehensive screening of genes resistant to an anticancer drug in esophageal squamous cell carcinoma. *International Journal of Oncology*. 2015;**47**(3):867-874
- [4] Mehdipour Moghaddam MJ, Mirbagheri AA, Salehi Z, Habibzade SM. Prevalence of class 1 integrons and extended spectrum beta lactamases among multi-drug resistant *Escherichia coli* isolates from North of Iran. *Iranian Biomedical Journal*. 2015;**19**(4):233-239
- [5] Knetsch MLW, Koole LH. New strategies in the development of antimicrobial coatings: The example of increasing usage of silver and silver nanoparticles. *Polymers*. 2011;**3**(1):340-366
- [6] Poole K. Mechanisms of bacterial biocide and antibiotic resistance. *Journal of Applied Microbiology*. 2002;**92**(S1):55-64
- [7] Jayaraman R. Antibiotic resistance: An overview of mechanisms and a paradigm shift. *Current Science*. 2009;**96**(11):1475-1484
- [8] Gurunathan S, Han JW, Dayem AA, Eppakayala V, Kim JH. Oxidative stress-mediated antibacterial activity of graphene oxide and reduced graphene oxide in *Pseudomonas aeruginosa*. *International Journal of Nanomedicine*. 2012;**7**:5901-5914
- [9] Zakharova OV, Godymchuk AY, Gusev AA, Gulchenko SI, Vasyukova IA, Kuznetsov DV. Considerable variation of antibacterial activity of Cu nanoparticles suspensions depending on the storage time, dispersive medium, and particle sizes. *BioMed Research International*. 2015;**2015**:412530, 1-11
- [10] Leung YH, Ng AM, Xu X, Shen Z, Gethings LA, Wong MT, et al. Mechanisms of antibacterial activity of MgO: Non-ROS mediated toxicity of MgO nanoparticles towards *Escherichia coli*. *Small*. 2013;**10**(6):1171-1183
- [11] Ramalingam B, Parandhaman T, Das SK. Antibacterial effects of biosynthesized silver nanoparticles on surface ultrastructure and nanomechanical properties of Gram-Negative bacteria viz. *Escherichia coli* and *Pseudomonas aeruginosa*. *ACS Applied Materials & Interfaces*. 2016;**8**(7):4963-4976
- [12] Lim JY, Yoon J, Hovde CJ. A brief overview of *Escherichia coli* O157:H7 and its plasmid O157. *Journal of Microbiology and Biotechnology*. 2010;**20**(1):5-14
- [13] Rasheed MU, Thajuddin N, Ahamed P, Teklemariam Z, Jamil K. Antimicrobial drug resistance in strains of *Escherichia coli* isolated from food sources. *Revista do Instituto de Medicina Tropical de São Paulo*. 2014;**56**(4):341-346
- [14] Taylor T, Unakal C. *Staphylococcus aureus*. 2nd ed. Treasure Island, FL: StatPearls Publishing; 2018
- [15] Bush L, Schmidt C, Perez M. Infecciones por *Staphylococcus aureus*—Infecciones—Manual

- MSD versión para profesional. 2018. Available from <https://www.msmanuals.com/es/hogar/infecciones/infecciones-bacterianas/infecciones-por-staphylococcus-aureus>; [Accessed: November 2018]
- [16] Kodoth V, Jones M. The effects of ultraviolet light on *Escherichia coli*. *Journal of Emerging Investigators*. 2015;**102**(3):23-28
- [17] Davis D. The History of Chitosan. 2018. Available from: <https://www.streetdirectory.com/etoday/the-history-of-chitosan-euolup.html> [Accessed: November 2018]
- [18] Choi C, Nam JP, Nah JW. Application of chitosan and chitosan derivatives as biomaterials. *Journal of Industrial and Engineering Chemistry*. 2016;**33**:1-10
- [19] Fernandez-Saiz P, Lagaron J, Ocio M. Optimization of the biocide properties of chitosan for its application in the design of active films of interest in the food area. *Food Hydrocolloids*. 2009;**23**(3):913-921
- [20] Sedaghat F, Yousefzadi M, Toiserkani H, Najafipour S. Bioconversion of shrimp waste *Penaeus merguensis* using lactic acid fermentation: An alternative procedure for chemical extraction of chitin and chitosan. *International Journal of Biological Macromolecules*. 2017;**104**:883-888
- [21] Muxika A, Etxabide A, Uranga J, Guerrero P, de la Caba K. Chitosan as a bioactive polymer: Processing, properties and applications. *International Journal of Biological Macromolecules*. 2017;**105**(2):1358-1368
- [22] Moura MJ, Brochado J, Gil MH, Figueiredo MM. In situ forming chitosan hydrogels: Preliminary evaluation of the in vivo inflammatory response. *Materials Science and Engineering C*. 2017;**75**:279-285
- [23] Ogawa Y, Azuma K, Izawa H, Morimoto M, Ochi K, Osaki T, et al. Preparation and biocompatibility of a chitin nanofiber/gelatin composite film. *International Journal of Biological Macromolecules*. 2017;**104**(B):1882-1889
- [24] Patil S, Nanduri L. Interaction of chitin/chitosan with salivary and other epithelial cells—an overview. *International Journal of Biological Macromolecules*. 2017;**104**(B):1398-1406
- [25] Elshaarawy R, Mustafa F, van Geelen L, Abou-Taleb A, Tadros H, Kalscheuer R, et al. Mining marine shell wastes for polyelectrolyte chitosan anti-biofoulants: Fabrication of high-performance economic and ecofriendly anti-biofouling coatings. *Carbohydrate Polymers*. 2017;**172**:352-364
- [26] Radtke A, Piszczek P, Topolski A, Lewandowska Ż, Talik E, Andersen IH, et al. The structure and the photocatalytic activity of titania based nanotube and nanofiber coatings. *Applied Surface Science*. 2016;**368**:165-172
- [27] Kudo A, Miseki Y. Heterogeneous photocatalyst materials for water splitting. *Chemical Society Reviews*. 2009;**38**(1):253-278
- [28] Polderman MC. New Applications of UVA-1 Cold Light Therapy. Doctoral thesis. Leiden University; 2006
- [29] Zheng M, Mingyuan G, Yanping J, Guoliang J. Preparation, structure and properties of TiO<sub>2</sub>-PVP hybrid films. *Materials Science and Engineering B*. 2000;**77**(1):55-59
- [30] Sayes CM, Wahi R, Kurian PA, Liu Y, West JL, Ausman KD, et al. Correlating nanoscale titania structure with toxicity: A cytotoxicity and inflammatory response study with human dermal fibroblasts and human

lung epithelial cells. *Toxicological Sciences*. 2006;**92**(1):174-185

[31] Blinova I, Ivask A, Heinlaan M, Mortimer M, Kahru A. Ecotoxicity of nanoparticles of CuO and ZnO in natural water. *Environmental Pollution*. 2010;**158**(1):41-47

[32] Davis R. Synthesis and characterization of VPI-5-supported titania clusters. *Chemistry of Materials*. 1992;**4**(6):1410-1415

[33] Welte A, Waldauf C, Brabec C, Wellmann PJ. Application of optical absorbance for the investigation of electronic and structural properties of sol-gel processed TiO<sub>2</sub> films. *Thin Solid Films*. 2008;**516**(20):7256-7259

[34] Wang L, Hu C, Shao L. The antimicrobial activity of nanoparticles: Present situation and prospects for the future. *International Journal of Nanomedicine*. 2017;**12**:1227-1249

[35] Hashimoto K, Irie H, Fujishima A. TiO<sub>2</sub> photocatalysis: A historical overview and future prospects. *Japanese Journal of Applied Physics*. 2005;**44**:8269-8285

[36] Leung S. Exposure to titanium dioxide and other metallic oxide nanoparticles induces cytotoxicity on human neural cells and fibroblasts. *International Journal of Nanomedicine*. 2008;**3**(4):533-545

[37] Zhukova LV. Evidence for compression of *Escherichia coli* K12 cells under the effect of TiO<sub>2</sub> nanoparticles. *ACS Applied Materials & Interfaces*. 2015;**7**(49):27197-27205

[38] Jung WK, Koo HC, Kim KW, Shin S, Kim SH, Park YH. Antibacterial activity and mechanism of action of the silver ion in *Staphylococcus aureus* and *Escherichia coli*. *Applied and Environmental Microbiology*. 2008;**74**(7):2171-2178

[39] Pan X, Wang Y, Chen Z, Pan D, Cheng Y, Liu Z, et al. Investigation of antibacterial activity and related mechanism of a series of nano-Mg(OH)<sub>2</sub>. *ACS Applied Materials & Interfaces*. 2013;**5**(3):1137-1142

[40] Sangari M, Umadevi M, Mayandi J, Pinheiro JP. Photocatalytic Degradation and Antimicrobial Applications of F-doped MWCNTs/TiO<sub>2</sub> Composites. *Spectrochimica Acta Part A: Molecular and Biomolecular Spectroscopy*. 2015;**139**:290-295

[41] Fourier Transform Infrared Spectroscopy (FT-IR) | NUANCE: Northwestern University Atomic and Nanoscale Characterization Experimental Center. 2018. Available from: <http://www.nuance.northwestern.edu/keck-ii/keck-ii-instruments/ftir-spectroscopy/index.html> [Accessed: November 2018]

[42] Causserand C, Aimar P. Characterization of filtration membranes. In: *Comprehensive Membrane Science and Engineering*. Oxford, UK: Elsevier. Vol. 1. 2010. pp. 311-335

[43] Bish DL, Post JE. *Modern Powder Diffraction*. Washington, DC: The Mineralogical Society of America; 2006

[44] Egerton RF. *Physical Principles of Electron Microscopy: An Introduction to TEM, SEM, and AEM*. US: Springer; 2005